Physicochem. Probl. Miner. Process., 57(6), 2021, 127-139

http://www.journalssystem.com/ppmp

Physicochemical Problems of Mineral Processing

ISSN 1643-1049

Received August 09, 2021; reviewed; accepted October 16, 2021

Mechanism and kinetics of pyrite transformation at elevated temperatures

Alvaro Aracena [1], Oscar Jerez [2]

[1] Escuela de Ingeniería Química, Pontificia Universidad Católica de Valparaíso, Avenida Brasil 2162, Valparaíso 2362854, Chile

[2] Instituto de Geología Económica Aplicada (GEA), Universidad de Concepción, Casilla 160-C, Concepción, Chile

Corresponding author: alvaro.aracena@pucv.cl (A. Aracena)

Abstract: Pyrite (FeS_2) is known as a sulfide that provides energy for various pyrometallurgical processes (fusion and conversion). There are several studies related to the evaluation of pyrite oxidation mechanisms at high temperatures, obtaining discrepancies in the products generated. In our work, the novelty of our research would be to obtain the thermochemical oxidation mechanism of FeS_2 by using conventional thermogravimetric methods. The oxidative roasting of pyrite from 550 to 800°C was analyzed for an oxygen concentration of 5.07 to 28.06 kPa of oxygen and particle size between 12.3 to 33.8 microns. The results showed that the pyrite proceeded by sequential roasting: first, it produced an intermediate compound, pyrrhotite (Fe_7S_8), which was later oxidized to generate hematite (Fe_2O_3), both stages validated by weight loss of the sample as well as by analysis by DRX. Each stage had a different roasting speed as it was also influenced differently by different parameters. The temperature and particle size favored the rate of pyrrhotite generation, and the oxygen concentration favored the rate of hematite formation. The first-order kinetic equation ln ($1-X_{Py}$) represented the roasting of the first stage ($FeS_2 \rightarrow Fe_7S_8$), with a calculated activation energy of 70.1 kJ/mol. The order of reaction was 0.5 concerning the partial pressure of oxygen and inversely proportional to the initial particle radius.

Keywords: pyrite, pyrrhotite, roasting, kinetics

1. Introduction

1.1. Usefulness of pyrite

Copper sulfide concentrates such as enargite (Cu_3AsS_4) and chalcopyrite ($CuFeS_2$) are accompanied by various compounds mainly consisting of pyrite (FeS_2), pyrrhotite (Fe_7S_8), among others. Iron sulfides are used to provide energy (in the form of heat) to thermal processes such as roasting and smelting of concentrates. Therefore, it is of relevance the knowledge of the parameters that exert a greater amount of energy as well as an acceleration in the oxidation rate of these compounds. One of these parameters is the calculation of the total equilibrium pressure of sulfur gas on pyrite validated from 325 to 743°C (Hong, 1998), given by the following expression:

$$\log_{10} P = 16.2(\pm 0.21) - \frac{15700(\pm 150)}{T} \quad (1)$$

where P is the total pressure of the sulfide gas over the pyrite (bar) and T is the temperature (kelvin). Otherwise, the melting point of FeS_2 is recorded as 743°C (Boyabat et al., 2004), while Fe_7S_8 would have a melting point given between a temperature range of 988 to 1187°C (Kubaschewski, 1982). These two values are so far not fully validated by the technical literature.

The chemical mechanisms governing the transformation of these sulfides are also of importance. However, there are several studies with different experimental techniques used that have shown discrepancies in the analyses above. Table 1 summarizes several investigations showing different results in the pyrite oxidation in similar ranges of oxygen concentrations and temperatures to generate different

DOI: 10.37190/ppmp/143124

compounds of non-stoichiometric pyrrhotite ($Fe_{(1-x)}S$), hematite (Fe_2O_3), magnetite (Fe_3O_4) or a mixture of them.

Table 1. Summary of research on oxidative pyrite roasting at different temperatures.

Total or partial reaction mechanism	Atmosphere/temperature condition	Maximum temperature	Reference
$FeS_2 \rightarrow Fe_2O_3$	Air (21% O_2 v/v)/2-6 K/min	T>480°C	(Schorr et al., 1969)
$FeS_2 \rightarrow Fe_2O_3$	Air (21% O_2 v/v)/2.5 K/min	T~503°C	(Dunn et al., 1989ab)
$FeS_2 \rightarrow Fe_2O_3$		T<515°C	
$FeS_2 \rightarrow Fe_2O_3$	O_2 concentration=2% v/v	T<800°C	(Groves et al., 1987)
$FeS_2 \rightarrow Fe_2O_3$ + traces Fe_3O_4		T>800°C	
$FeS_2 \rightarrow FeS_2 + Fe_{(1-x)}S \rightarrow Fe_2O_3$	O_2 concentration=5% v/v	T=525°C	(Hansen, 2003)
$FeS_2 \rightarrow Fe_3O_4 \rightarrow Fe_2O_3$	O_2 concentration=1-5% v/v	T=700-900°C	(Nishihara and Kondo, 1959)
$FeS_2 \rightarrow Fe_3O_4$ (>85%) + Fe_2O_3	O_2 concentration=3% v/v	T=1227°C	(Srinivasachar et al., 1990)
$FeS_2 \rightarrow Fe_3O_4$ + traces Fe_2O_3	O_2 concentration=5% v/v	T=1038-1454°C	(Huffman et al., 1989)
$FeS_2 \rightarrow Fe_2O_3$	Air (21% O_2 v/v)	T<550°C	(Jorgensen and Moyle, 1982)
$FeS_2 \rightarrow Fe_{(1-x)}S \rightarrow Fe_2O_3$		T>550°C	
$FeS_2 \rightarrow Fe_2O_3$ + traces Fe_3O_4	Air (21% O_2 v/v)	T=610°C	(Prasad et al., 1985)
$FeS_2 \rightarrow Fe_{(1-x)}S \rightarrow Fe_2O_3$			
$FeS_2 \rightarrow Fe_{(1-x)}S \rightarrow Fe_3O_4$			
$FeS_2 \rightarrow FeS$	Air (21% O_2 v/v)	T=173-261°C	(Mitovski et al. 2015)
$FeS \rightarrow Fe_3O_4$ $FeS \rightarrow Fe_2O_3$		T=275-596°C	
$FeS_2 \rightarrow FeO + Fe_2O_3 + Fe_3O_4$	O_2 concentration variable	T=1200-1600°C	(McLennan et al., 2000)
$Fe_{(1-x)}S \rightarrow FeO \rightarrow Fe_3O_4 \rightarrow Fe_2O_3$	Reducing atmosphere		
$FeS_2 \rightarrow Fe_{(1-x)}S$	O_2 concentration=100-1000 ppm + CO_2	T=484-538°C	(Hong and Fegley, 1997)
$FeS_2 \rightarrow Fe_{(1-x)}S + Fe_3O_4$		T=392-460°C	
$FeS_2 + C \rightarrow Fe_2O_3 + Fe_3O_4$ (lower amounts)	Air (21% O_2 v/v)	T=300-757°C	(Komraus et al., 1990)
$FeS_2 + 2CO_2 \rightarrow Fe_3O_4 + Fe_2O_3 + COS_{(g)} + SO_2$	CO_2 atmosphere	T>500°C	(Bhargava et al., 2009)
$FeS_2 \rightarrow Fe_3O_4 + Fe_2O_3$	O_2 concentration variable + pulverized coal	T=1227°C	(Helble et al., 1990)

In summary, it can be seen from the table that pyrite oxidation to form hematite is generated above 480°C up to 800°C, according to four studies (Schorr and Everhart, 1969; Dunn et al., 1989ab; Groves et al., 1987). This oxidation occurred for an atmosphere of 21% oxygen. In another study (Hansen, 2003), when working within the above temperature range, lowering the oxygen concentration to 5% v/v, non-stoichiometric pyrrhotite appeared as a result. In parallel, another author (Jorgensen and Moyle, 1982) indicated that non-stoichiometric pyrrhotite would be produced (experimentally evidenced) depending on the temperature for O_2=21% concentration. On the other hand, author (Prasad et al., 1985) commented that pyrite would oxidize and thermally decompose depending on the experimental conditions for the same temperature (610°C), within the range used by (Schorr and Everhart, 1969), (Dunn et al., 1989ab; Groves et al., 1987; Jorgensen and Moyle, 1982), at O_2=21% concentration. On the contrary, for very high temperatures (above 700°C), pyrite would oxidize to form various oxidized iron compounds within a range of oxygen concentrations (between 1-5% O_2) (Huffmanet al., 1989; Srinivasachar et al., 1990; Nishihara and Kondo, 1959; McLennan et al., 2000). Unfortunately, hematite appears as trace amounts, but in another study, it is an important part resulting from oxidation. When working at very low temperatures (T<270 ° C), pyrrhotite appears, but then there is a generation of iron oxides at high temperatures (Mitovski et al., 2015). When a reducing atmosphere (carbon or CO_2) is

used, different oxidized compounds are produced at temperatures above 1200°C. Non-stoichiometric pyrrhotite occurs at very low temperatures (392 to 538°C) (Hong, 1997), but in a parallel study (McLennan, 2000), pyrrhotite appeared at elevated temperatures (1200°C). However, in three studies where coal and carbon dioxide atmosphere were used to generate the reducing atmosphere (Komraus et al., 1990; Helble et al., 1990; Bhargava et al., 2009) there was no evidence of the pyrrhotite compound, only oxidized iron compounds,

Based on the information gathered from the technical literature presented so far, the present investigation aims to obtain the reaction mechanisms as well as the pyrite oxidation kinetics at temperatures above 500°C for an oxygen-nitrogen mixture atmosphere.

1.2. Physicochemical behaviour of pyrite

Predominance diagrams summarizing the thermochemical reactions are used to understand the physicochemical behavior of pyrite oxidation. These diagrams predict the stability or instability of sulfide species in contact with vapor phases in roasting or smelting processes. Fig. 1 shows the diagram of the Fe-S-O system at a temperature of 650°C showing the condensed species Fe, FeS_2, Fe_7S_8, $FeSO_4$, and Fe_2O_3 which are in equilibrium with the vapor phase as a function of S_2 and O_2 partial pressure. The lines in the diagram separate the stability fields of the condensed phases. The thermochemical data used to generate the diagram were obtained from the HSC Chemistry program database (HSC Chemistry, 1999)

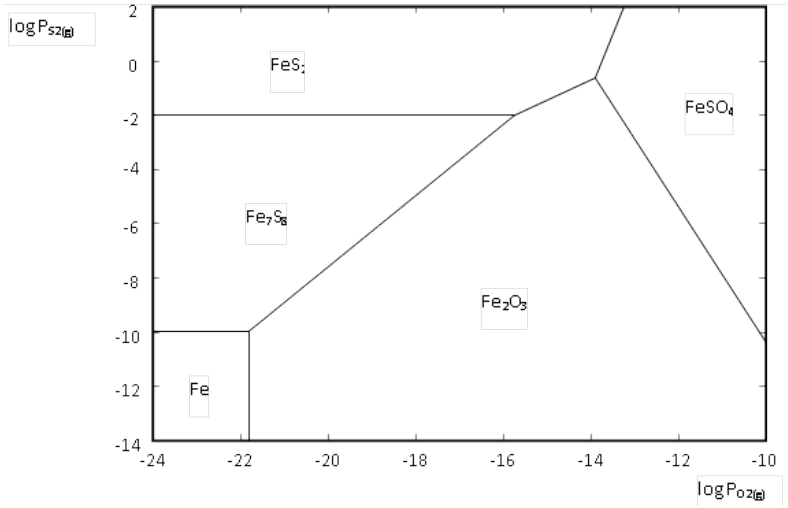

Fig. 1. Stability diagram of the Fe-S-O system at 650°C

In the diagram it can be predicted that in the absence of oxygen (log P_{O2}<-16) a first thermochemical reaction translated into a thermal decomposition of pyrite to produce pyrrhotite would be generated, being more likely that this decomposition occurs compared to the oxidation of pyrite to produce hematite, because the equilibrium line between these two condensed phases (FeS_2/Fe_7S_8) is much widespread compared to the line between FeS_2/Fe_2O_3. On the other hand, by increasing the oxygen concentration in the gas phase, the pyrrhotite would be oxidized to generate hematite. Therefore, pyrite would proceed from two possible transformation mechanisms which would be thermal decomposition with an intermediate compound (Fe_7S_8) and finally with the generation of the oxidized compound, Fe_2O_3.

2. Experimental methods

2.1. Pyrite samples

All experiments were carried out with samples of pyrite concentrates from the flotation process, obtained from the Andina-Codelco Chile Division mine. These concentrates were dried and classified into four average particle size fractions: 12.3, 16.0, 22.7, and 33.8 microns. Most of the experiments were conducted with an average particle size of 16 microns. Based on chemical analysis, the iron content was

45.6%. An X-ray diffraction (XRD) analysis of the 16.0 microns sample showed major pyrite peaks (Fig. 2), with no significant presence of any other compounds. With these two results, the calculated FeS_2 content was 97.85%.

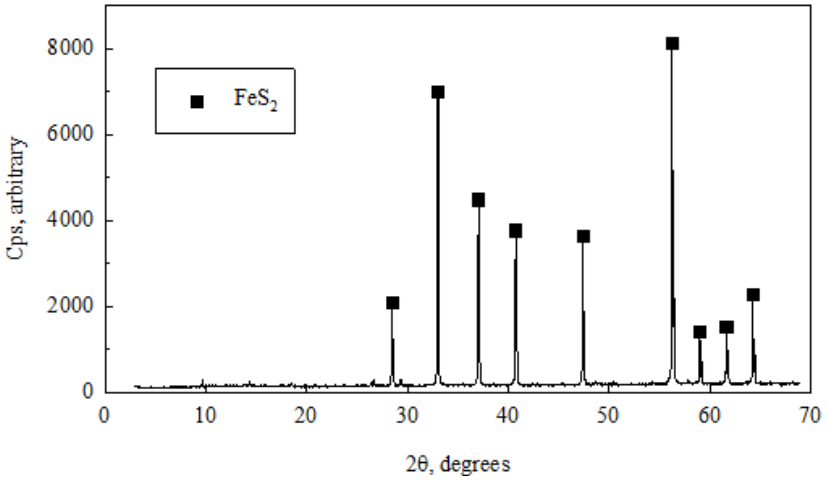

Fig. 2. Diffractogram of the initial pyrite concentrate sample

2.2. Thermogravimetric system

The experiments were carried out by the weight loss measurement method in a conventional thermogravimetric apparatus. This apparatus can be seen in Fig. 3. It basically consisted of a vertically

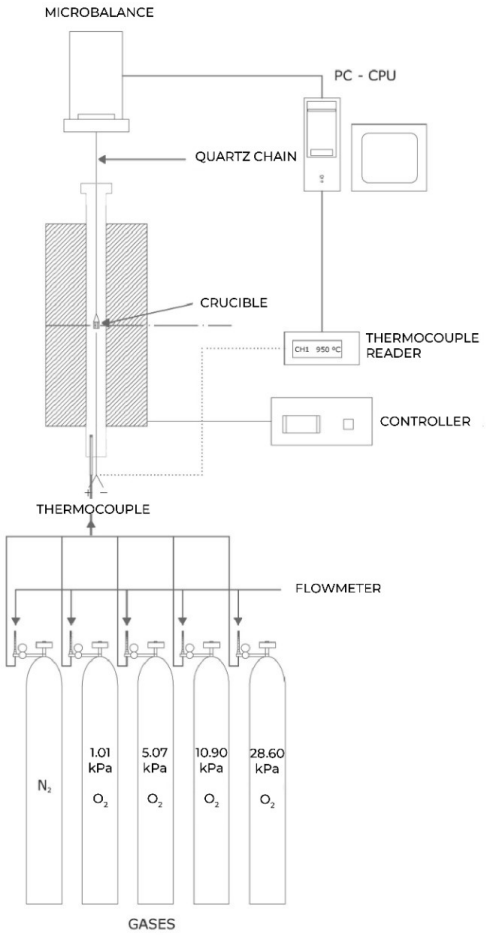

Fig. 3. Configuration of the thermogravimetric equipment with the gas train

placed quartz tube mounted in a vertical oven with controllable temperature. The sample temperature was measured by a chromel/alumel thermocouple placed in the constant temperature region in the reaction tube, which was a space of about 90 mm in the center of the tube. A microbalance with a sensitivity of 0.00001 g was placed on the furnace tube, additionally, a data acquisition system, and a gas distribution system designed to provide nitrogen-oxygen atmospheres of various compositions. The thermogravimetric system was verified by testing coal of known chemical composition in a neutral atmosphere (101.3 kPa nitrogen) and different oxidizing atmospheres to validate the system. This carbon validation procedure has already been used in previous work (Aracena et al., 2016ab).

2.3. Experimental procedure

The samples used were placed in a 1.3 mL ceramic crucible (11 mm internal diameter (ID)×14 mm height (H)). In most experiments, approximately 50 mg of pyrite sample was placed in the crucible where it was introduced into the preheated reaction tube and suspended from the microbalance by a quartz chain in the constant temperature region of the tube. Every three seconds the weight loss of the sample was recorded.

After the experimental time had elapsed, the solid samples were removed from the furnace. They were then rapidly cooled by injecting a high flow of nitrogen over the crucible, which lasted for a cooling time of about 20 seconds. The samples were moved to a desiccator and then sent to XRD to identify the crystalline compounds possibly generated. In some experiments, partially reacted samples were obtained in time ranges when changes were visualized in the slopes of the weight loss curves where possible intermediate compounds could exist during the oxidation process.

3. Results and discussion

3.1. Preliminary experiments

Some preliminary experiments were carried out to evaluate the effect of the reaction gas flow rate (between 0.5 to 1.7 L/min) that could affect the mass transfer of pyrite roasting above 500°C. For this purpose, 50 mg of pyrite sample with a particle size of 16 microns was used. The oxidizing atmosphere was 10.90 kPa oxygen and had a temperature of 600°C. Fig. 4 shows a summary of the results. The data are plotted as the sample weight loss fraction given as ΔW/Wo, where ΔW is equal to (Wo-Wt) where Wo is the initial sample weight and Wt is the sample weight at time t.

It can be seen in Fig. 4 that the reaction gas flow did not have a preponderant effect on the pyrite oxidation rate. Therefore, when having a thin layer of pyrite solid sample inside the crucible, the role of mass transfer resistance was not significant for these working conditions. Hence, for the following experiments, it was decided to work with 50 mg of sample and a reaction flow rate of 1.0 L/min. All experiments were conducted isothermally and at constant oxygen partial pressure.

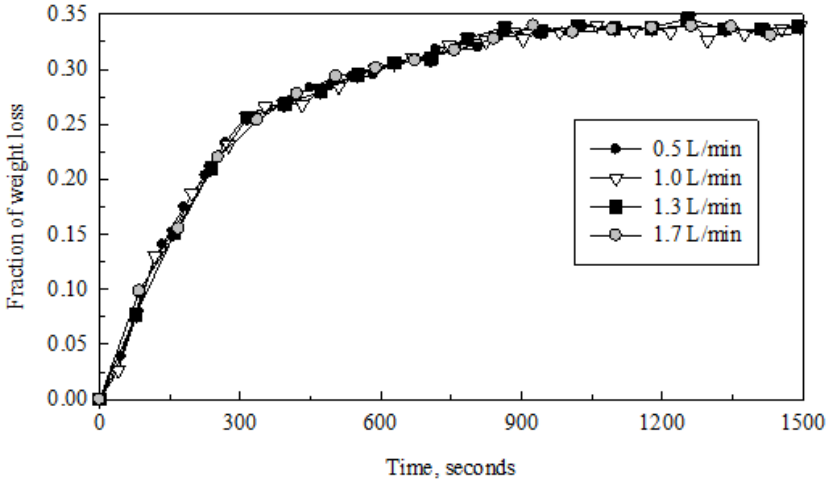

Fig. 4. Pyrite weight loss fraction as a function of time for different reaction gas flow rates for a temperature of 600°C and atmosphere of 10.90 kPa oxygen

3.2. Pyrite reaction mechanisms for temperature above 500°C

Some preliminary experiments were developed to evaluate the temperature ranges. According to Aracena (2016b) pyrite when oxidized from 400 to 500°C promotes the generation of the oxide, hematite. In our experiments, 50 mg of pyrite with a particle size of 16 microns was used, taking contact at oxygen partial pressure of 10.90 kPa and temperatures of 600 and 800°C. A 500°C curve was also added. Fig. 5 shows the summary of the experimental results.

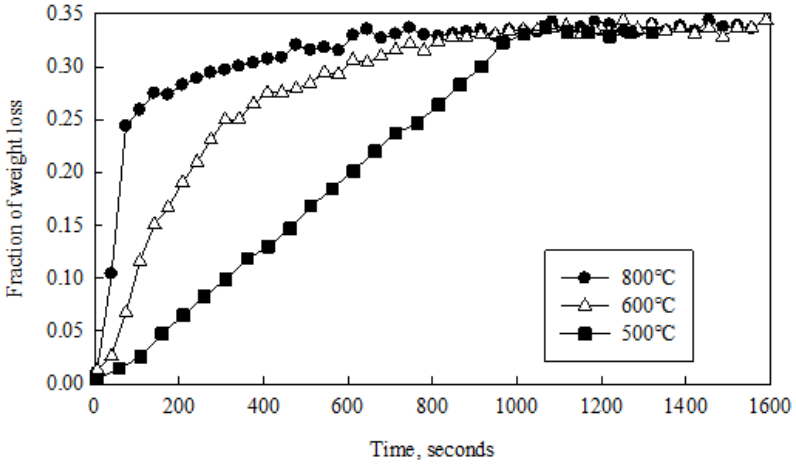

Fig. 5. Effect of temperature on pyrite reaction mechanisms in oxidizing atmosphere (10.90 kPa oxygen)

The curves obtained at 500, 600, and 800°C reach a maximum value of 0.33 weight loss fraction. This same value was recorded in previous work (Aracena, 2016b). The theoretical weight loss fraction represents the complete oxidation of pyrite to hematite, according to reaction (2). However, for the case of temperatures higher than 500°C, two different slopes can be observed before reaching complete oxidation, a case that was not observed in the curve at 500°C, nor in the previous study (Aracena, 2016b). These curves have slope changes close to a value of 0.23 in weight loss fraction and then reach a maximum value of 0.33. To elucidate the possible reaction mechanisms, partially and fully reacted samples were obtained from annex experiments using the same conditions of 600°C and O_2 partial pressure of 10.90 kPa for times of 160, 600, and 1300 seconds, representing a weight loss fraction of 0.15, 0.30, and 0.33, respectively. The three samples were sent for XRD analysis. The results are shown in Fig. 6, where it can be observed that at 160 seconds (Fig. 6-A) pyrite diffraction lines could be identified as well as a new sulfide, a type of pyrrhotite (Fe_7S_8). No oxidized iron compounds were visible in this diffractogram. At 600 seconds (Fig. 6-B), lines of pyrrhotite and the oxidized compound, hematite, are observed, without the presence of pyrite. At the end of the roasting time, 1300 seconds (Fig. 6-C), only hematite diffraction lines were observed, with no sulfide identified. These results would demonstrate that the oxidation of pyrite at temperatures above 500°C proceeds by the formation of an intermediate compound, such as pyrrhotite (first stage of roasting), which in turn this second sulfide would oxidize to generate hematite (second stage of roasting). For the formation of Fe_7S_8, it would be produced by thermal decomposition of pyrite, due to the absence of oxides in the solids. Reaction (3) represents the generation of pyrrhotite where oxygen acts on gaseous sulfur to form SO_2. Reaction (4) represents the oxidation of Fe_7S_8 to hematite.

As observed in Fig. 5, the first curve goes up to an experimental weight loss fraction of 0.23. The theoretical weight loss fraction of Fe_7S_8 generation from FeS_2 (reaction 3) is 0.23. This data agrees with that observed in Fig. 5 for a temperature of 600°C and 800°C where the slope change occurs. The same is presented with the theoretical fraction of oxidation of pyrite to hematite (reaction 2) which goes to a value of 0.33. This reaction would be the overall pyrite roasting process, also reported by Aracena (2016b), for temperatures below 500°C.

The impact of demonstrating these new pyrite roasting mechanisms is focused on the amount of energy that each proposed reaction can deliver, which would generate a thermal balance inside a roasting reactor. Furthermore, in kinetic terms, each reaction (3 and 4) could have its own roasting

velocity being affected independently of the same study factors, generating a better use of the reaction time in the same reactor. The latter will be discussed later.

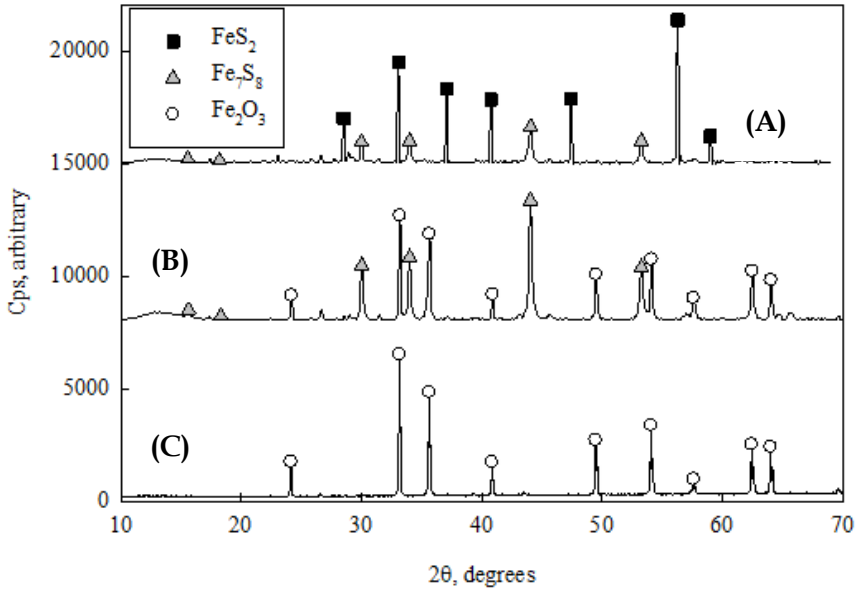

Fig. 6. Diffractogram of partially and fully reacted samples

$$FeS_2 + 11/4O_{2(g)} \rightarrow 1/2Fe_2O_3 + 2SO_{2(g)} \quad (2)$$

$$7FeS_2 + 6O_{2(g)} \rightarrow Fe_7S_8 + 6SO_{2(g)} \quad (3)$$

$$2Fe_7S_8 + 53/2O_{2(g)} \rightarrow 7Fe_2O_3 + 16SO_{2(g)} \quad (4)$$

3.3. Effect of temperature on the oxidation of pyrite

The effect of temperature on the overall oxidation of pyrite in an atmosphere of 5.07 kPa oxygen in the temperature range of 550°C to 800°C and 16.0 microns size was investigated. Fig. 7 shows the pyrite oxidation rate as the fraction of sample weight loss versus reaction time. It can be seen that temperature has a preponderant effect on the oxidation of pyrite as well as pyrrhotite (slope changes). When the temperature is increased, the rate of the first stage of roasting was influenced more significantly than the second stage. Thus, a weight-loss fraction of 0.20 is achieved in 520 seconds at 550°C, whereas, at a temperature of 800°C, the same weight fraction is reached in 38 seconds, 13.7 times faster. However, regarding the second stage, for a fraction of 0.31 it is achieved in 1420 seconds (550°C) while increasing the temperature (800°C), the same fraction is obtained in 530 seconds, only 2.7 times faster.

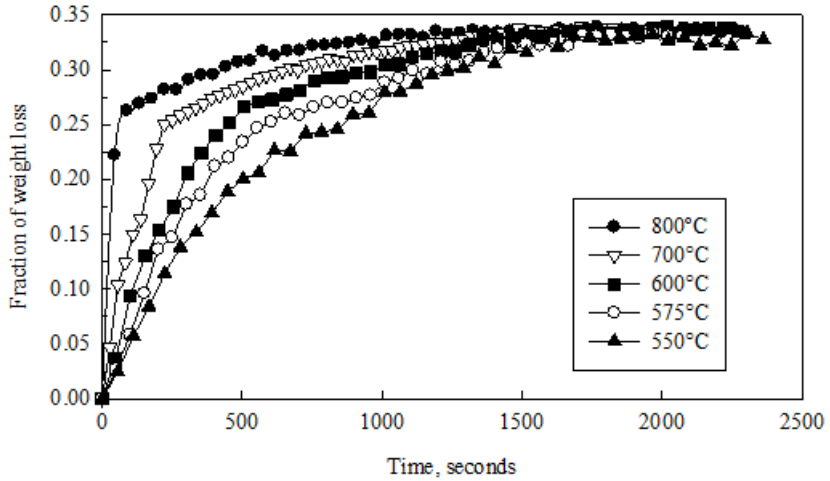

Fig. 7. Pyrite weight loss curves for temperature ranges from 550 to 800°C for an oxygen concentration of 5.07 kPa

The strong temperature dependence of the first stage of pyrite oxidation would be an indication that the thermal decomposition of pyrite would be controlled by the chemical reaction on the surface of the particle. On the other hand, the second stage (oxidation of pyrrhotite to hematite) would be controlled by the molecular diffusion of oxygen gas through the porous layer formed.

3.4. Oxygen concentration effect

The effect of oxygen concentration on the pyrite roasting rate was analyzed for a temperature of 600°C in the range of 5.07 to 28.60 kPa oxygen (Fig. 8). It can be observed that, by increasing the oxygen concentration, the pyrite roasting rate to pyrrhotite increases as well as towards hematite generation. The opposite is the case concerning the phenomenon given for the temperature analysis. The effect of oxygen is pronounced with the second stage ($Fe_7S_8 \rightarrow Fe_2O_3$) compared to the first stage ($FeS_2 \rightarrow Fe_7S_8$). In this first stage, as it would be controlled by the chemical reaction, the influence of the oxygen concentration does not promote a greater effect, contrary to what was observed for the second stage.

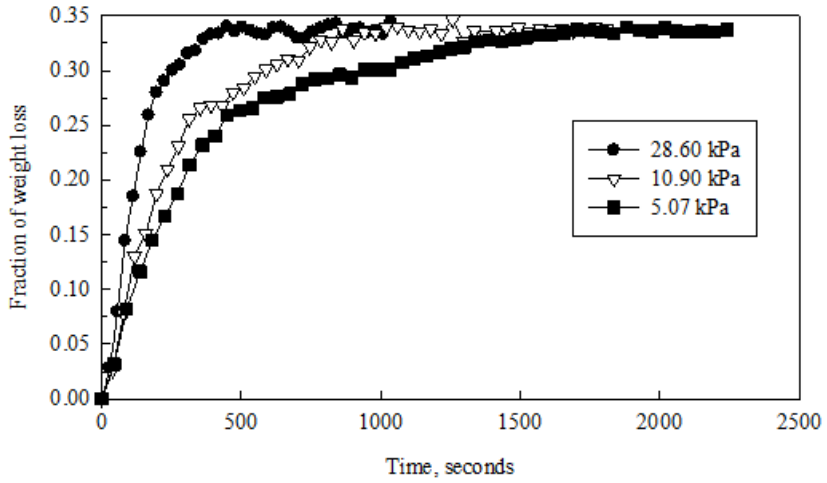

Fig. 8. Effect of oxygen concentration on pyrite roasting rate for a temperature of 600°C.

Related work on the FeS_2 roasting process (under 500°C) at 28.60 kPa indicated that the amount of oxidized pyrite decreased to a fraction of 0.18 (Aracena, 2016) as the temperature decreased. This occurred because hematite formation generated an outer layer preventing pyrite oxidation. In this investigation (above 500°C), XRD samples were obtained at an oxygen concentration of 28.60 kPa and a time of 900 seconds (not shown in this research). The results showed only hematite peaks, with no sulfide found (neither pyrite nor pyrrhotite). This showed that the pyrite roasting was complete and only hematite was generated, contrary to what happened when roasting is obtained below 500°C.

3.5. Particle size effect

Fig. 9 shows the results obtained for different pyrite particle sizes (12.3, 16.0, 22.7, and 33.8 microns) for a concentration of 5.07 kPa of oxygen and temperatures of 800 and 600°C. It can be observed that particle size has a preponderant effect on the first stage of pyrite roasting compared to the second stage. For temperatures of 600°C, as the particle size decreases, the pyrite decomposition rate increases. On the contrary, this decrease in size did not influence the oxidation of pyrrhotite to hematite, obtaining similar roasting rates. These two phenomena can be validated by the limiting stages that would govern both stages, the first would be by chemical reaction and the second by diffusion. When a temperature of 800°C was used, the first stage is very fast as the particle size increased, however, for the second stage, pyrrhotite oxidation rates are maintained.

The reaction mechanisms established in this research, as well as the factors that influence the speed of transformation and generation of sulfurized/oxidized iron species, have added the technical literature presented here (Table 1). However, the depth of this updated study given by thermogravimetry techniques and subsequent validation have shown that there are two half-reactions

over 550°C and at different oxygen concentrations, completely different cases from those shown in Table 1.

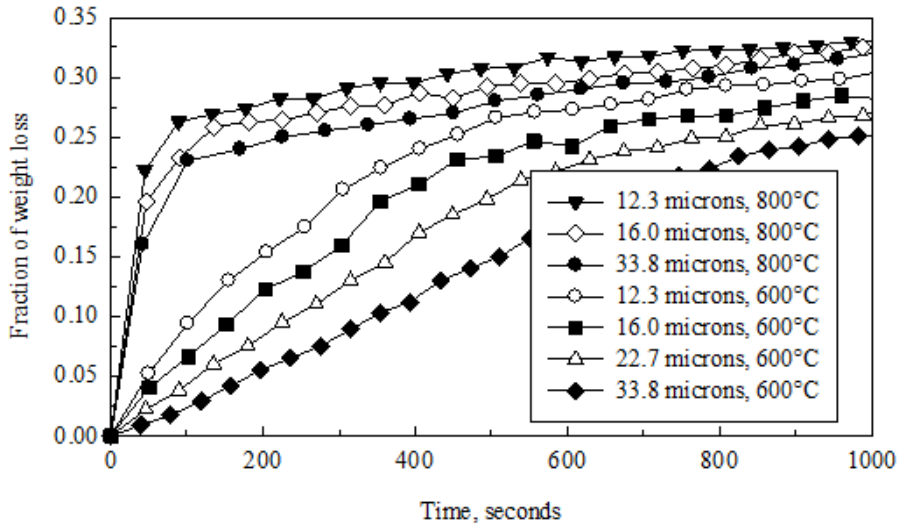

Fig. 9. Evaluation of particle size on pyrite roasting rate for the two stages of formation: pyrrhotite and hematite in an atmosphere of 5.07 kPa O_2

3.6. Oxidation kinetics of pyrite to pyrrhotite

As discussed, the first stage of the reaction (equation 3) would be relevant because it is the first transformation that pyrite undergoes to consolidate its oxidation completely. According to Fig. 7, no change in the thermal decomposition reaction mechanism of pyrite to pyrrhotite is shown. Therefore, it is reasonable to promote that the sample underwent a uniform internal reaction, and the reaction products diffuse easily. Under these conditions, the first stage of pyrite thermal decomposition reaction can be represented by a simple model assuming control by chemical reaction. The following first-order kinetic equation regarding the fraction converted would fit the experimental data very well:

$$\ln(1 - X_{Py}) = k_{app} t \tag{5}$$

where X_{Py} is the fraction converted from FeS_2 to Fe_7S_8, k_{app} is the apparent reaction rate constant, and t is the time. The apparent rate constant will depend on temperature, gas phase concentration, and average particle size. The dependence of these factors can be determined from the following equation:

$$k_{app} = k \frac{b(P_{O_2})^n}{r_o} e^{-\frac{E_a}{RT}} \tag{6}$$

Here, k is the intrinsic kinetic constant, b is the stoichiometric coefficient given by equation (3), where is the molar ratio between oxygen molecules and pyrite particles, P_{O2} and n is the partial pressure and reaction order concerning oxygen, r_o is the average particle radius, E_a is the activation energy, R is the gas constant and T is the temperature.

Using the experimental data in Fig. 7, a plot was constructed that will represent the chemical reaction model as a function of time for the temperature range 550 to 800°C. Fig. 10 shows the results of a good linear fit of the experimental data with regression coefficients (R^2) above 0.99 for the entire temperature range. These high R^2 values validate the kinetic equation (5). The apparent reaction rate constants (the slopes of each straight line) are presented in Table 2.

Like what was developed previously, the reaction order "n" was obtained using the experimental data given in Fig. 8 where the k_{app} values (the slopes of each straight line) as a function of time for the different oxygen partial pressures could be extracted using equation (5). The results are summarized in Fig. 11. The linear fit of the experimental data and the chosen model can be observed. The k_{app} values were used to construct the graph ln k_{app} as a function of ln P_{O2} which is presented in Fig. 12. In this figure, the linear fit of the apparent kinetic constant values with R^2 over 0.98 can be observed. The reaction order n was calculated using the slope value which resulted in a value of 0.5 with respect to the oxygen partial pressure.

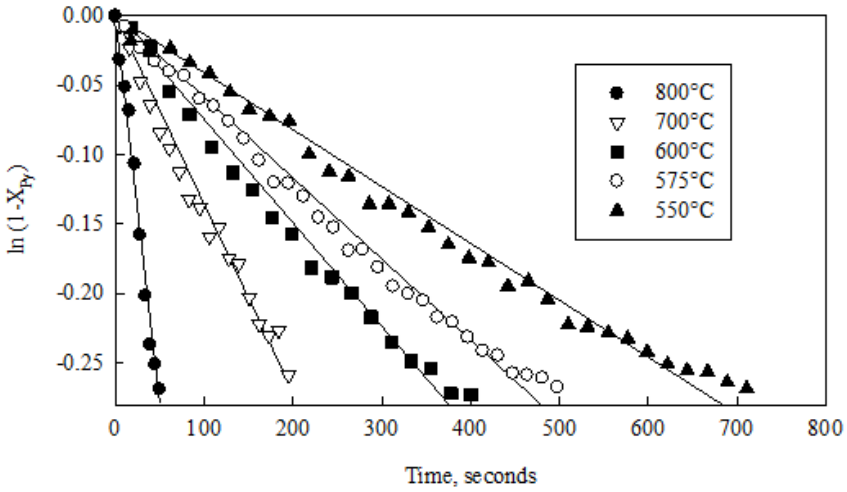

Fig. 10. First order kinetics of pyrite oxidation to produce pyrrhotite at P_{O2}=5.07 kPa

Table 2. For each temperature studied, the values obtained for the apparent rate constants are shown

T,°C (K)	1000/T, 1/K	$k_{app}\times10^4$, 1/s
550 (823)	1.2151	4.28
575 (848)	1.1792	5.86
600 (873)	1.1455	7.55
700 (973)	1.0277	13.74
800 (1073)	0.9320	55.70

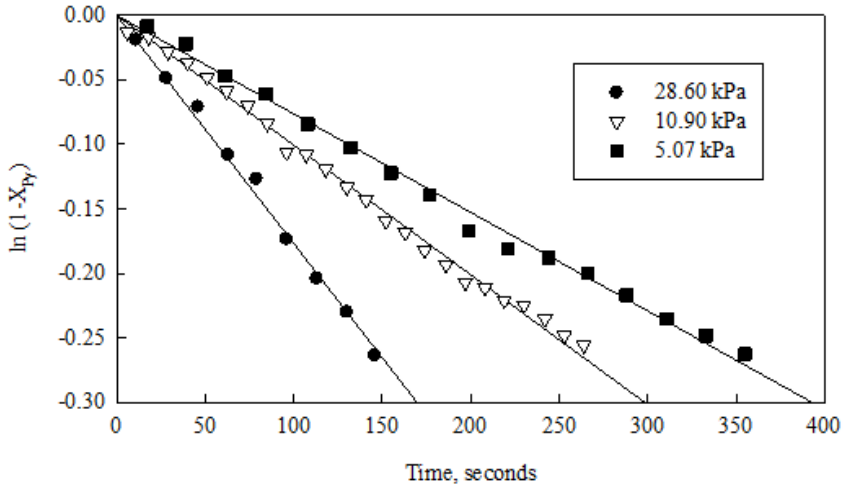

Fig. 11. ln (1-X_{Py}) as a function of time and oxygen partial pressure in the oxidation of pyrite to pyrrhotite at 600°C

Observing equation (6), the particle radius varies inversely with the apparent kinetic constant. To corroborate this relationship, the experimental data in Fig. 9 were used, fitted to equation (5), and Fig. 13 was constructed. It can be seen that relationship ln (1-X_{Py}) complies very well with the experimental data generating a good fit for all four particle sizes. The k_{app} values obtained from this figure were plotted in Fig. 14 as a function of the inverse of the initial particle radius for a temperature of 600°C. The linear dependence of these values shown in the figure (R^2>0.99) supports the kinetic model used for this case.

Next, to obtain the activation energy (E_a), one must first calculate the intrinsic kinetic oxidation constant, k, for the different temperatures using the apparent kinetic constants obtained from Fig. 10. The value of n will be 0.5 and the stoichiometric constant of b will be 6/7 according to reaction (3). The particle size used was 16.0 microns and oxygen concentration of 5.07 kPa. The calculated values of the intrinsic constants were used to draw the Arrhenius diagram shown in Fig. 15. This figure shows a good

linear fit (R^2>0.95) for the apparent kinetic constants for each temperature. The calculated activation energy was 70.1 kJ/mol for the temperature range 550-800°C, which is the typical value for a chemical reaction-controlled reaction.

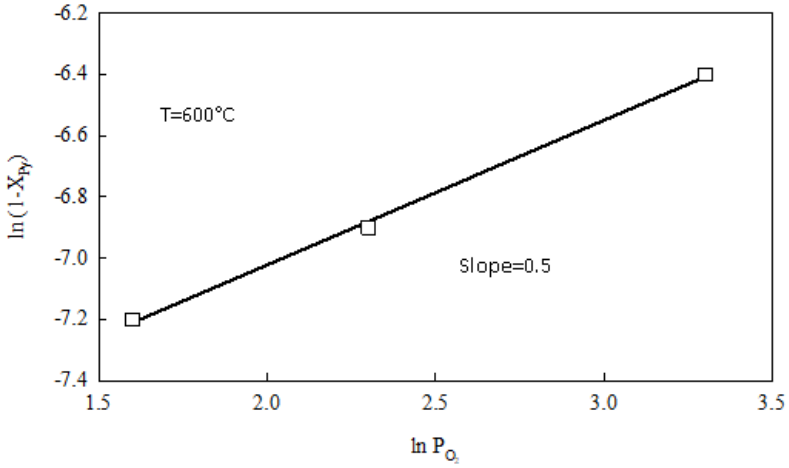

Fig. 12. Dependence of the apparent reaction rate constant on oxygen partial pressure

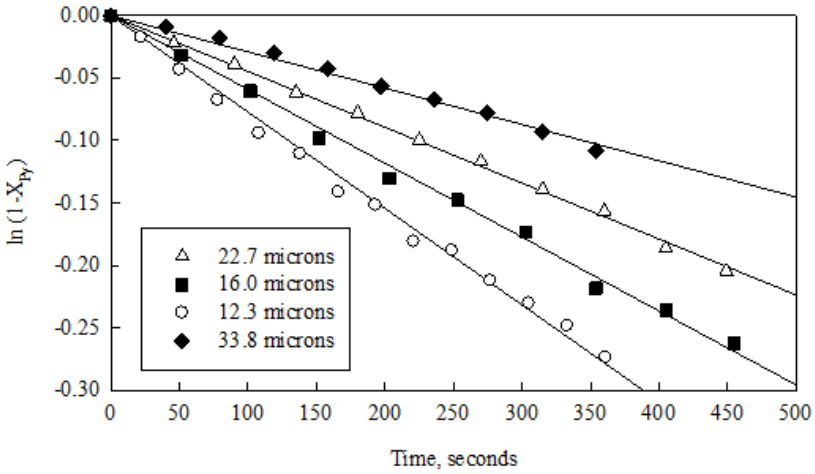

Fig. 13. Kinetics of pyrite to pyrrhotite roasting for different particle sizes

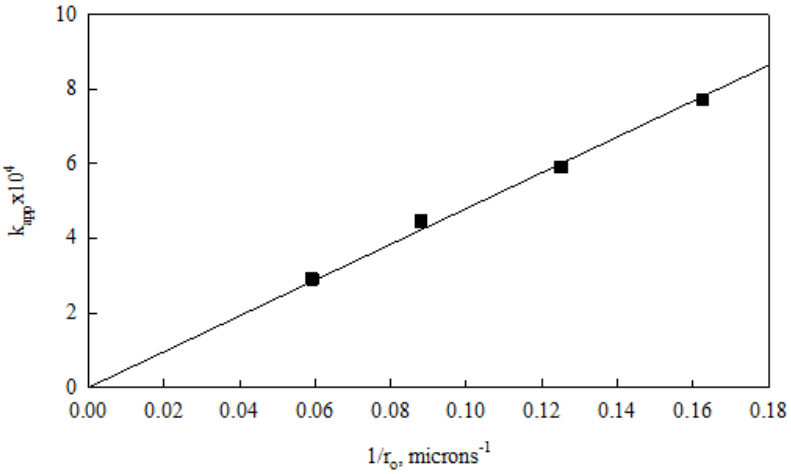

Fig. 14. Dependence of the apparent kinetic rate constant of the oxidation of pyrite to pyrrhotite on the inverse of the initial particle size

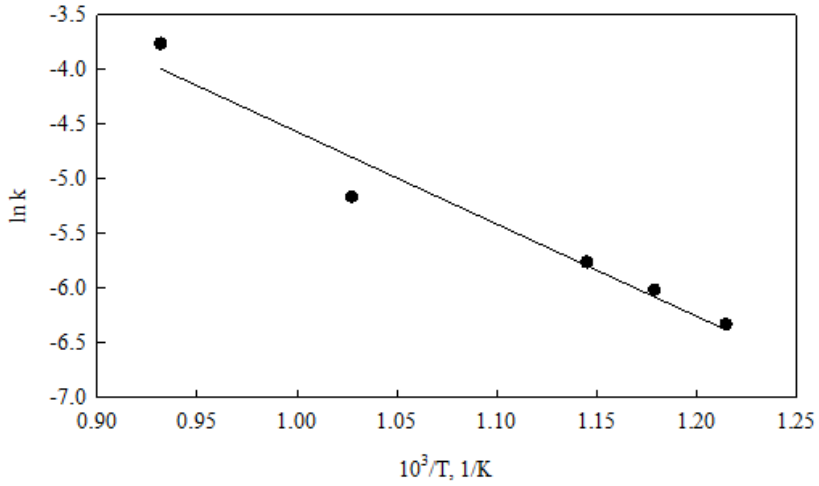

Fig. 15. Arrhenius plot for the temperature range from 550 to 800°C

Therefore, the oxidation kinetics of pyrrhotite in an oxygen-containing atmosphere can be represented by the following expression:

$$\ln\left(1-X_{Py}\right)=4.77\times10^{7}\,\frac{{}^{6}/_{7}\,(P_{O_2})^{0.5}}{r_o}\,e^{-\frac{70100}{RT}}t \tag{7}$$

where R equals 8.314 J mol^{-1} K^{-1}, r_o is in microns, (P_{O2}) is in kPa, t is in seconds and k=4.77×10^{7} µm kPa$^{-0.5}$ s^{-1}.

4. Conclusions

Pyrite was sequentially oxidized over 500°C, generated pyrrhotite (first stage), pyrrhotite was oxidized to finally form hematite (second stage). These oxidation mechanisms were thermodynamically evaluated and experimentally validated by sample weight loss and XRD analysis.

In kinetic terms, the increase in temperature favored the first stage over the second stage, otherwise with the effect of oxygen concentration, which produced a decrease in oxidation time in the second stage. By decreasing the particle size, it generated a positive increase in the roasting speed of the first stage.

The model that best represented the roasting of the first stage ($FeS_2 \rightarrow Fe_7S_8$) was ln (1-$X_{Py}$), with a calculated activation energy of 70.1 kJ/mol. The order of reaction was 0.5 concerning the partial pressure of oxygen and inversely proportional to the initial particle radius.

Acknowledgments

A.A. and O.J. thank ANID FONDECYT INICIACIÓN, 11180432 project.

References

ARACENA, A., JEREZ, O., ANTONUCCI, C., 2016a. *Senarmontite volatilization kinetics in nitrogen atmosphere at roasting/melting temperatures*, Transactions of Nonferrous Metals Society of China, 26, 294-300.

ARACENA, A., JEREZ, O., ORTIZ, R., MORALES, J., 2016b. *Pyrite oxidation kinetics in an oxygen-nitrogen atmosphere at temperatures from 400 to 500°C,* Canadian Metallurgical Quarterly, 55, 195-201.

BHARGAVA, S.K., GARG, A., SUBASINGHE, N.D., 2009. *In situ high-temperature phase transformation studies on pyrite*, Fuel, 88, 988-993.

BOYABAT, N., ÖZER, A.K., BAYRAKCEKEN, S., GÜLABOGLU, M.S., 2004. *Thermal decomposition of pyrite in the nitrogen atmosphere.* Fuel Process Technol, 85, 179–88.

DUNN, J.G., DE, G.C., O'CONNOR, B.H., 1989a. *The effect of experimental variables on the mechanism of the oxidation of pyrite: Part 1. Oxidation of particles less than 45 µm in size*. Thermochim Acta, 145, 115-130.

DUNN, J.G., DE, G.C., O'CONNOR, B.H., 1989b. *The effect of experimental variables on the mechanism of the oxidation of pyrite: Part 2. Oxidation of particles of size 90–125 µm*. Thermochim Acta, 155, 135-149.

GROVES, S.J., WILLIAMSON, J., SANYAL, A., 1987. *Decomposition of pyrite during pulverized coal combustion*, Fuel, 66, 461-466.

HANSEN, J.P., 2003. *SO_2 Emissions from Cement Production*. PhD Thesis, Department of Chemical Engineering, Technical University of Denmark.

HELBLE, J.J., SRINIVASACHAR, S., BONI, A.A., 1990. *Factors influencing the transformation of minerals during pulverized coal combustion,* Progress in Energy and Combustion Science, 16, 267-279

HONG Y., FEGLEY, B., 1997. *The kinetics and mechanism of pyrite thermal decomposition*. Ber. Bunsen. Phys. Chem., 101, 1870-1881.

HONG, Y., FEGLEY, B., 1998. *The sulfur vapor pressure over pyrite on the surface of Venus*. Planet and Space Science, 46, 683–90.

HSC Chemistry, version 6.0, OutoKumpu Research Py: Pori, Finland, 1999.

HUFFMAN, G. P., HUGGINS, F.E., LEVASSEUR, AA., 1989. *Investigations of the transformations of pyrite in a droptube furnace*. Fuel, 68, 485-490.

JORGENSEN, F., MOYLE, F.J., 1982. *Phases formed during the thermal analysis of pyrite in air*, Journal of Thermal Analysis, 25, 473-485.

KOMRAUS, J.L., POPIEL, E.S., MOCEK, R., 1990. *Chemical transformations of ferruginous minerals during the process of oxidation of hard coal*. Hyperfine Interact, 58, 2589-2592.

KUBASCHEWSKI, O., 1982. *Iron-binary phase diagrams. Iron–sulphur*. Berlin: Springer, pp. 125.

MCLENNAN, A.R., BRYANT, G.W., STANMORE, B.R., WALL, T.F., 2000. *Ash formation mechanisms during of combustion in reducing conditions*, Energy Fuels, 14, 150-159.

MITOVSKI, A., STRBAC, N., MANASIJEVIC, D., SOKIC, M., DAKOVIC, A., ZIVKOVIC, D., BALANOVIC, Lj., 2015. *Thermal analysis and kinetics of the chalcopyrite-pyrite concentrate oxidation process,* Metalurgija, 54, 311-314.

NISHIHARA, K., KONDO, Y., 1959. *Studies of the oxidation of Pyrite I, II and III*. Mem Fac. Eng., Kyoto Univ., 21, 214-218.

SCHORR, J.R., EVERHART, J.O., 1969. *Thermal behavior of pyrite and its relation to carbon and sulfur oxidation in clays.* Journal of the American Ceramic Society, 52, 351-354.

PRASAD, A., SINGRU, R.M., BISWAS, A.K., 1985. *Study of the roasting of pyrite minerals by Mössbauer spectroscopy*, Physical Status Solidi A, 87, 267-271.

SRINIVASACHAR, S., HELBLE, J.J., BONI, A.A., 1990. *Mineral behavior during coal combustion 1. Pyrite transformation*, Progress in Energy and Combustion Science, 16, 281-292.